RSC Advances

PAPER

Cite this: *RSC Adv.*, 2016, **6**, 63933

DNA assembly of silicon quantum dots/gold nanoparticle nanocomposites†

Asuka Inoue,[a] Hiroshi Sugimoto,[a] Hidenobu Yaku[b] and Minoru Fujii*[a]

Received 25th May 2016
Accepted 24th June 2016

DOI: 10.1039/c6ra13565j

www.rsc.org/advances

Silicon quantum dots (Si-QDs) dispersible in water and exhibiting bright near infrared (NIR) luminescence are a very attractive nano-light-emitter usable in bioimaging and biosensing. Here, we demonstrate the fabrication of NIR luminescent nanocomposites composed of Si-QDs and gold nanoparticles (Au-NPs) by DNA hybridization. We first develop processes to functionalize the surface of Si-QDs with different types of silane coupling agents without notably affecting the water solubility and the luminescence properties, and then conjugate the functionalized Si-QDs with single-stranded DNA (ssDNA). DNA hybridization with a Au-NP with complementary ssDNA results in the formation of Si-QDs/Au-NP nanocomposites.

Semiconductor quantum dots (QDs) with size-tunable photoluminescence (PL) have been intensively studied as nanoprobes for biomedical applications[1–4] due to the suitable chemical and photophysical properties compared to organic dyes and fluorescent proteins.[5] However, toxic heavy metal elements in commercially available CdX and PbX (X = S, Se and Te) QDs raise concern for their application in biomedical fields. Silicon (Si) QDs are considered to be a promising alternative to the CdX and PbX QDs because of the high biocompatibility and biodegradability.[6,7]

Numerous efforts have been made to develop water-dispersible and brightly luminescent Si-QD targeting for biomedical applications.[6–18] In the development of Si-QDs, a crucial step is the functionalization of the surface with biomolecules such as proteins and nucleic acids.[18–21] Jonghoon *et al.* achieved coupling of streptavidin with Si-QDs using a multistep photoassisted reaction.[18] Wang *et al.* conjugated 1–2 nm diameter Si-QDs to DNA through formation of a carboxamide bond.[19] Romuald *et al.* reported conjugation of Si-QDs with DNA by pulsed laser ablation in liquid.[20] In these previous work, the luminescence wavelength is in the 400–600 nm range,[18–21] which is much shorter than that commonly reported for hydrogen or oxygen terminated Si-QDs.[22,23] The mechanism of the short wavelength shift by organic capping is still controversial.[24–30] For the application of biomolecule-functionalized Si-QDs in bioimaging and biosensing, the emission wavelength is preferably within the transparent window of tissues (700–1000 nm).[31]

One of the purposes of this work is to develop biomolecule-functionalized Si-QDs exhibiting PL in the NIR range. We employ B and P codoped all-inorganic Si-QDs as a starting material.[32] The codoped Si-QDs have negative surface potential and are dispersible in water almost perfectly without organic ligands.[33] They exhibit size tunable and stable PL in the NIR range in water.[33] First, we functionalize the surface by three types of silane coupling agents *via* the surface Si–OH bonds and study the influence on the solution dispersibility and the PL properties. We then conjugate Si-QDs and single-stranded DNA (ssDNA) and demonstrate the formation of nanocomposites composed of Si-QDs and gold (Au) nanoparticles (NPs) by DNA hybridization. By this process, the distance between Si-QDs and Au-NPs can be controlled with high accuracy. We also show the formation of similar structures by using Au–S bonding.

First, we briefly summarize the structural and optical properties of B and P codoped all-inorganic Si-QDs used in this work. The size of the Si-QDs can be controlled by the growth temperature (T_a) in a wide energy range (0.9–1.85 eV).[34] In this work, we employ two samples grown at 1150 and 1200 °C. Note that the structural and chemical properties of the two samples are almost identical except for the luminescence wavelength. Fig. 1(a) shows the optical transmittance spectra of water solutions of codoped Si-QDs grown at 1150 and 1200 °C. In both samples, the transmittance in the NIR range is almost 100%, indicating that Si-QDs are perfectly dispersed in water. In fact, from the photograph in Fig. 1(b), the solution is very clear and characters behind the bottle can clearly be seen. The high water dispersibility is due to the negative surface potential (zeta potential: ~−35 mV at pH 7) and electrostatic repulsion between QDs.[32] Fig. 1(c) shows a transmission electron microscope (TEM) image of Si-QDs grown at 1150 °C. For the TEM

[a]*Department of Electrical and Electronic Engineering, Graduate School of Engineering, Kobe University, Rokkodai, Nada, Kobe 657-8501, Japan. E-mail: fujii@eedept.kobe-u.ac.jp*

[b]*Advanced Research Division, Panasonic Corporation, 3-4, Hikaridai, Seika-cho, Souraku-gun, Kyoto, 619-0237, Japan*

† Electronic supplementary information (ESI) available: Details are shown in Fig. S1–3. See DOI: 10.1039/c6ra13565j

observations, the water solution is dropped on a carbon-coated Cu mesh. Si-QDs are aligned two dimensionally and no three-dimensional agglomerates are observed. The average diameter (d_{ave}) is 4.8 nm with the standard deviation of 1.4 nm (Fig. 1(d)). In the high-resolution image in the inset, lattice fringes corresponding to {111} planes of Si crystal (0.314 nm) can be seen. The TEM image and the size distribution of Si-QDs grown at 1200 °C are shown in Fig. 1(e) and (f), respectively. In this case, the average diameter is 6.7 nm and the standard deviation is 1.2 nm.

Fig. 1(g) shows infrared (IR) absorption spectra of codoped Si-QDs grown at 1150 and 1200 °C stored in methanol for about two months after preparation. A major peak around 1080 cm^{-1} is Si–O–Si stretching mode. Small peaks around 1300–1500 cm^{-1} and 2100–2200 cm^{-1} are assigned to B–O–B stretching and Si–H stretching modes, respectively. Note that, just after preparation, the surface is mainly H-terminated,[35] and oxidation slowly proceeds during storage in methanol. After a month of storage in methanol, the surface is dominated by Si–O bonds.

Fig. 1(h) shows the PL spectra of codoped Si-QDs in water. Depending on the size, the PL wavelength is changed from 900 to 1000 nm. It should be noted that the PL wavelengths are longer than those of conventional Si-QDs with comparable sizes.[34] The long wavelength shift is due to the formation of donor and acceptor states in the band gap by B and P codoping.[34]

For the surface functionalization, we use surface Si–O bonds, which are abundant after storage in methanol (Fig. 1(g)), to functionalize Si-QDs. In order to introduce amino and thiol groups onto the surface *via* the Si–O bonds, 3 different types of silane coupling agents, (A) (3-mercaptopropyl) trimethoxysilane, (B) (3-ethoxydimethylsilyl) propylamine and (C) (3-aminopropyl) trimethoxysilane, are employed (Fig. 2). First, 10 μl of silane coupling agent was added to methanol solution of Si-QDs (200 μl). The concentration of Si-QDs was 0.3 mg ml^{-1}, while that of silane coupling agent was chosen so that the number ratio of the molecules per a Si-QD becomes 250, 500

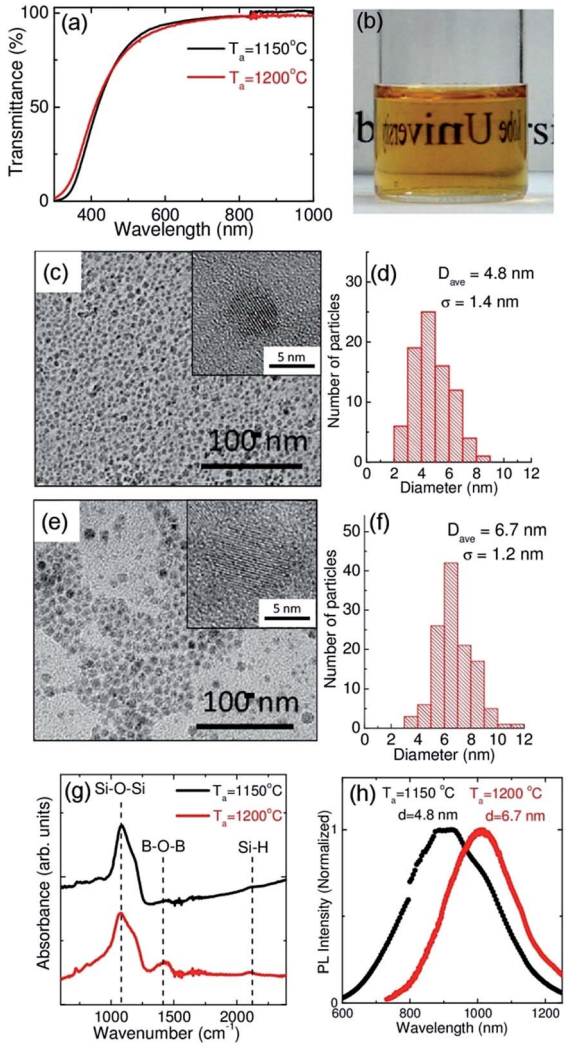

Fig. 1 (a) Optical transmittance spectra of water solutions of B and P codoped Si-QDs (T_a = 1150, 1200 °C). (b) Photograph of Si-QDs-dispersed water (T_a = 1200 °C). (c) TEM image and (d) size distribution of Si-QDs grown at 1150 °C. The inset shows a high resolution TEM image. (e) TEM image and (f) size distribution of Si-QDs grown at 1200 °C. The inset shows a high resolution TEM image. (g) IR absorption spectra of B and P codoped Si-QDs (T_a = 1150, 1200 °C) after storage in methanol for about 2 months. (h) Normalized PL spectra of codoped Si-QDs (T_a = 1150, 1200 °C).

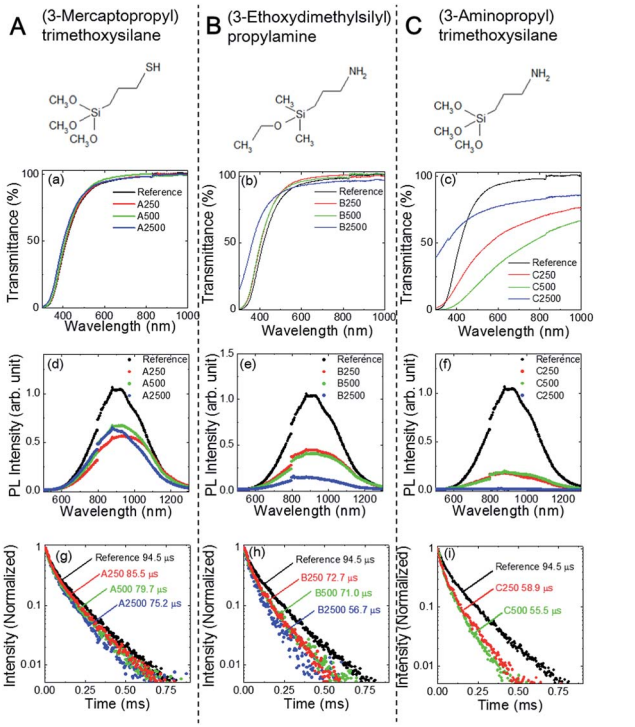

Fig. 2 (a)–(c) Optical transmittance spectra, (d)–(f) PL spectra excited at 405 nm, and (g)–(i) PL decay curves of Si-QDs (T_a = 1150 °C) functionalized by three kinds of molecules, (A) (3-mercaptopropyl) trimethoxysilane, (B) (3-ethoxydimethylsilyl) propylamine and (C) (3-aminopropyl) trimethoxysilane (detected at 890 nm). The nominal numbers of molecules per a Si-QD are 250 (red), 500 (green) and 2500 (blue). The data of untreated Si-QDs are shown by black symbols. All the measurements are performed in water.

and 2500. Hereafter, we distinguish samples with a symbol representing the molecules (A, B and C in Fig. 2) and the number ratio, *e.g.*, A250. After mixing, 10 μl of deionized (DI) water was added and sonicated for 30 min to promote hydrolysis. To remove unreacted molecules, the solution was filtered using Amicon Ultra-0.5 centrifugal filter units (3 kDa cut-off) (Millipore) at 14 000*g* for 30 min and Si-QDs collected on the filter were dispersed in DI water. The procedure was repeated twice. Finally, the solution was heated at 70 °C for 15 min to enhance covalent bonding of silane coupling agent with Si-QDs.[36–40]

Fig. 2(a)–(c) shows optical transmittance spectra of aqueous solution of functionalized Si-QDs ($T_a = 1150$ °C). In the case of (3-mercaptopropyl) trimethoxysilane (A250-A2500), the water dispersibility of Si-QDs is not degraded and the spectra are identical to that of untreated Si-QDs (black curve). In the case of (3-ethoxydimethylsilyl) propylamine (B250-B2500), the situation is slightly different. The transmittance spectrum changes slightly in the highest mixing ratio (B2500). This is due to agglomeration of Si-QDs and partial precipitation to the bottom. The precipitation is very serious in (3-aminopropyl) trimethoxysilane (C250-C2500). Even in the smallest mixing ratio (C250), the transmittance spectrum is completely different from that of the untreated ones.

The different behaviour between A and others (B and C) is explained by the kinds of functional group. Thiol group in A keeps the dispersibility, while amino group in B and C induces agglomeration. The difference can be explained by the surface potential. As described above, the surface of codoped Si-QDs is negatively charged. Functionalization by negatively charged thiol group enhances the surface charges and keeps Si-QDs dispersible in water. On the other hand, positively charged amino group cancels negative surface charges of Si-QDs and weakens the electrostatic repulsion between Si-QDs. Within B and C, more serious agglomeration in C can be explained by the larger number of silanol group, *i.e.*, 3 per a molecule instead of 1 per a molecule in B. The larger amount of silanol group makes cross linking of Si-QDs possible, which promotes the agglomeration.

In many of previous work on organic functionalized Si-QDs, PL properties are strongly modified by the functionalization process.[24–28,30,41] Quite often red to NIR emission disappears and blue or green emission appears after functionalization. This is not the case in this work. The PL spectra of all the samples are summarized in Fig. 2(d)–(f), together with the decay curves (Fig. 2(g)–(i)). In all the cases, the PL spectral shape is not affected by the functionalization. The extremely high insensitiveness of the PL properties on the functionalization process is a characteristic feature of B and P codoped Si-QDs. It should be stressed here that comparison of PL intensities between samples is not straightforward due to precipitation of Si-QDs in some samples.

In contrast to the PL intensity, the PL lifetime is not strongly affected by the degree of the agglomeration. In A, the lifetime is slightly shortened, which is accompanied by the intensity decrease. This suggests that non-radiative processes are introduced by the functionalization process, although they are not very serious considering the small degree of the PL quenching. The lifetime shortening and PL quenching are slightly larger in B. It may be possible that positive charges of the amino group affect the PL properties. Note that the strong decrease of the PL intensity in B2500 is not merely due to the introduction of non-radiative processes, but simply due to precipitation of QDs to the bottom. In C, the lifetime shortening and the quenching is more serious than others.

In order to confirm successful functionalization of Si-QDs surface, we produce nanocomposites of Si-QDs and Au-NPs by using thiol functionalized Si-QDs. Since thiol group forms chemical bonds with Au, nanocomposites are expected to be formed spontaneously by simply mixing aqueous solution of thiol functionalized Si-QDs ($T_a = 1150$ °C) with citrate-stabilized Au-NPs ($d_{ave} = 40$ nm) in diameter. Fig. 3(a) and (b) shows TEM images of the nanocomposites. The high-resolution TEM images are shown in Fig. 3(c) and (d). The dark regions about 40 nm in diameter are Au-NPs. Si-QDs are attached to the surface of the Au-NPs as confirmed by the high-resolution TEM images. Fig. 3(e) shows the energy-dispersive X-ray spectroscopy (EDS) mapping of a nanocomposite. We can clearly see that Au-NPs are surrounded by Si. The TEM observations and the EDS

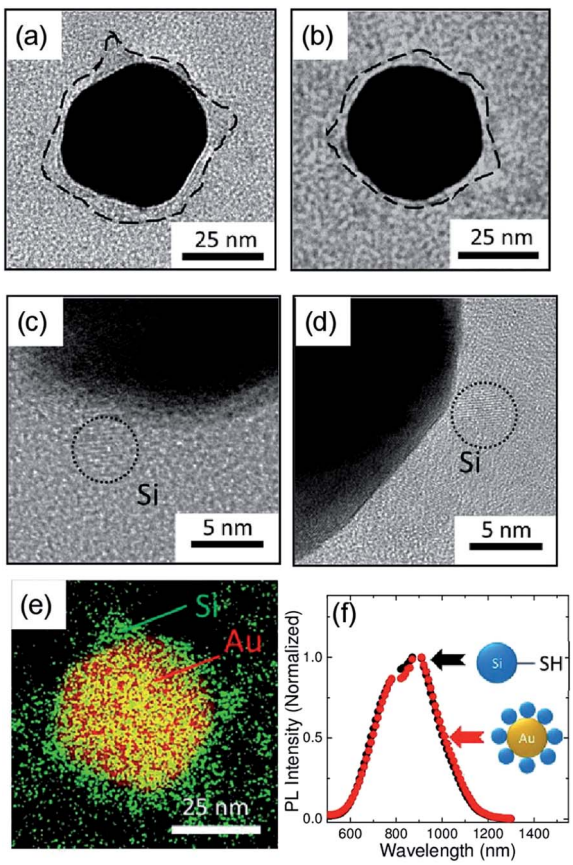

Fig. 3 (a), (b) TEM images, (c), (d) high-resolution TEM images and (e) STEM-EDS element mapping of a Si-QDs/Au-NP nanocomposite formed by Au–S bonds by using thiol terminated Si-QDs (T_a = 1150 °C). (f) Normalized PL spectra of thiol terminated Si-QDs (black) and Si-QDs/Au-NP nanocomposites (red). The excitation wavelength is 365 nm.

mapping confirm the formation of nanocomposites. Note that the size and shape of Au-NPs are not modified by the composite formation process (see ESI, Fig. S1(a),† a TEM image of a Au-NP before the composite formation). Fig. 3(f) shows the PL spectra of the nanocomposites. The spectral shape is almost identical with that of Si-QDs before the composite formation. It should be stressed here that the nanocomposites were not formed when untreated Si-QDs were used. This indicates that they are formed by the Au–S bonds.

Now we proceed to self-assembly of nanocomposites *via* DNA hybridization. The procedure is schematically shown in Fig. 4(a). First, amine terminated Si-QDs (T_a = 1200 °C) and carboxyl-modified ssDNA are conjugated by peptide bonding using 4-(4,6-dimethoxy-1,3,5-triazin-2-yl)-4-methylmorpholium chloride (DMT-MM) as a condensing agent.[42] The Si-QDs are then annealed with Au-NPs (d_{ave} = 80 nm) having the complementary ssDNA in hybridization buffer (ESI Fig. S1(b)†). Fig. 4(b)–(e) show the TEM images of the nanocomposites. The high resolution TEM images around the surface of Au-NPs are shown in Fig. 4(f)–(i). A STEM-EDS element mapping is shown in Fig. 4(j). The TEM images and a STEM-EDS mapping are similar to those in Fig. 3, and the formation of nanocomposites can clearly be recognized. In the ESI (Fig. S2†), STEM-EDS mappings of individual elements, *i.e.*, Au, N and Si, are shown. The N mapping image confirms the nanocomposite formation by DNA hybridization. An important difference from the case of Au–S bonding in Fig. 3 can be seen in the high-resolution TEM images. In Fig. 4(f)–(i), Si-QDs are indicated by circles and the distance between Si-QDs and Au-NPs is shown in the images. In contrast to Fig. 3, where Si-QDs are almost directly attached on the surface of Au-NPs, there are distances between Si-QDs and Au-NPs in Fig. 4. The distance is

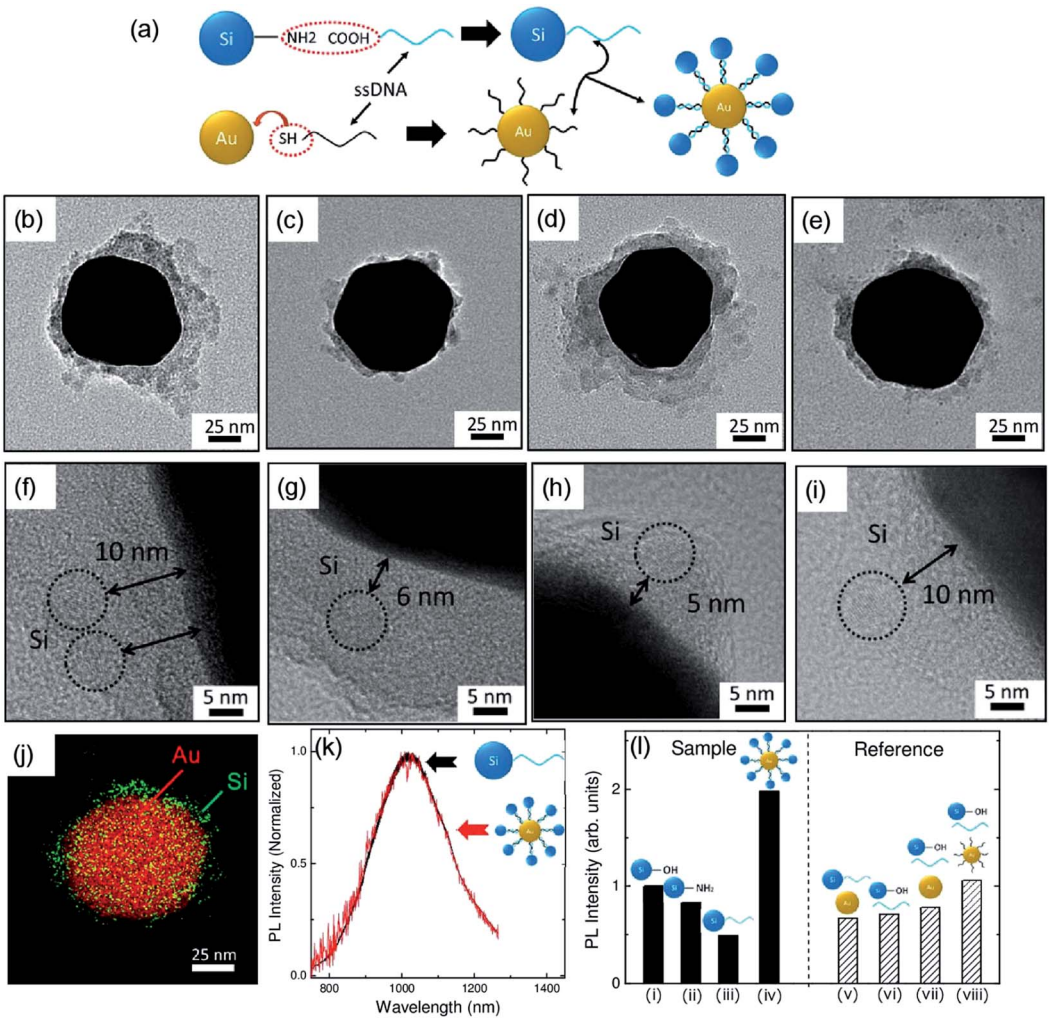

Fig. 4 (a) Schematic illustration of the fabrication process of Si-QDs/Au-NP nanocomposites (T_a = 1200 °C) by DNA hybridization. (b)–(e) TEM images, (f)–(i) high-resolution TEM images and (j) STEM-EDS element mapping of a Si-QDs/Au-NP nanocomposite formed by DNA hybridization. (k) Normalized PL spectra of thiol terminated Si-QDs (black) and Si-QDs/Au-NP nanocomposites (red). The excitation wavelength is 405 nm. (l) Summary of the evolution of the PL intensity during the nanocomposites formation process in solution. (i) Untreated Si-QDs, (ii) functionalization by amino group, (iii) conjugation with ssDNA and (iv) Si-QDs/Au-NP nanocomposites by DNA hybridization. (v)–(viii) Are control samples, (v) ssDNA conjugated Si-QDs and citrate-stabilized Au-NPs, (vi) untreated Si-QDs and ssDNA, (vii) untreated Si-QDs, ssDNA and citrate-stabilized Au-NPs and (viii) untreated Si-QDs, ssDNA and DNA functionalized Au-NPs.

distributed from 3.5 to 10 nm. The distribution is probably due to the fact that TEM image is a two-dimensional projection of a three dimensional object and the longest distance corresponds to the situation that a Si-QD is attached in the equatorial plane of a Au-NP. The longest distance coincides with the length of DNA used in the work (10 nm). This is a clear evidence that the nanocomposites are formed by DNA hybridization. Fig. 4(k) compares PL spectra before and after the DNA hybridization. The spectral shape is again not modified by the nanocomposite formation.

In Fig. 4(l), the evolution of the PL intensity during the whole process is summarized. Functionalization of the surface by amino group decreases the PL intensity by 20% ((ii) in Fig. 4(l)). By conjugation with ssDNA, the intensity drops to almost half of the initial value ((iii) in Fig. 4(l)). The intensity goes up by DNA hybridization ((iv) in Fig. 4(l)). The PL enhancement is considered to be due to the coupling with surface plasmons in Au-NPs,[43–46] although more detailed analyses including theoretical modelling is necessary for detailed understanding of the enhancement mechanism.

On the right side of Fig. 4(l), the PL intensities of several control samples are shown, *i.e.*, mixture of (v) ssDNA conjugated Si-QDs and citrate-stabilized Au-NPs, (vi) untreated Si-QDs and ssDNA, (vii) untreated Si-QDs, ssDNA and citrate-stabilized Au-NPs and (viii) untreated Si-QDs, ssDNA and DNA functionalized Au-NPs. Although the PL intensities are slightly different between them, all of them have much smaller PL intensity than that of the DNA-assembled nanocomposites. This supports surface plasmon enhanced fluorescence in the nanocomposites.

In conclusion, we have succeeded in producing water dispersible and NIR luminescent Si-QDs functionalized by thiol and amino groups. By using thiol functionalized Si-QDs, Si-QDs/Au-NP nanocomposites, in which Si-QDs are attached to the surface of Au-NPs, are formed. We also developed ssDNA conjugated Si-QDs by using amino group functionalized Si-QDs, and succeeded in fabricating Si-QDs/Au-NP nanocomposites by DNA hybridization. In the DNA-assembled nanocomposites, the distance between Si-QDs and Au-NPs are precisely controlled by the length of DNA. The development of nanocomposites composed of environmentally friendly Si-QDs by DNA hybridization pave the way for designing more complicated Si-QDs-based composites or hybrid structures useful for biosensing such as DNA detection with very high accuracy and controllability.

Experimental procedure

Preparation of B and P codoped Si-QDs

B and P codoped Si-QDs were prepared by the previously reported procedure.[47] Briefly, Si-rich boronphosphosilicate glass (BPSG) films were deposited on a stainless steel substrates by a co-sputtering method. The films were peeled from the plates and ground into powder, and then annealed in a N_2 gas atmosphere at 1150 and 1200 °C for 30 min, which results in the growth of B and P codoped Si-QDs about 5 and 7 nm in diameters, respectively. The annealed powder was etched by hydrofluoric acid (HF) solution (46 wt%), and codoped Si-QDs were extracted from the BPSG matrices. Finally, isolated Si-QDs were transferred to methanol and stored.

Preparation of ssDNA conjugated Si-QDs

Carboxyl-modified ssDNA at the 5′ end was purchased from Tsukuba Oligo Service Co., Ltd.,. The sequence was 5′-TCGTGTTCCCATCTGGTCCAGGTTTCGTGC-3′.[48] The ssDNA and amine terminated Si-QDs were conjugated by peptide bonding using DMT-MM as dehydrating agent. DMT-MM solution was added to amine terminated Si-QDs solution, then incubated for 4 h at room temperature.[42] The solution was filtered using Amicon Ultra-0.5 centrifugal filter units (3 kDa cut-off) (Millipore) at 14 000*g* for 30 min. Finally, ssDNA conjugated Si-QDs were dispersed in DI water.

Preparation of citrate stabilized Au-NPs and ssDNA conjugated Au-NPs

Citrate-stabilized Au-NPs (d_{ave} = 40 nm) (see a TEM image Fig. S1(a) in the ESI†) were fabricated by seeded growth synthesis.[49] For the preparation of ssDNA conjugated Au-NPs, thiol-modified ssDNA at the 5′ end was purchased from Tsukuba Oligo Service Co., Ltd. The sequence was 5′-GCA-CGA-AAC-CTG-GAC-CAG-ATG-GGA-ACA-GCA-3′, which was complementary to the ssDNA immobilized onto Si-QDs. The sequence is the same as that used in ref. 48. The conjugation of Au-NPs (d_{ave} = 80 nm) with the thiol-modified ssDNA was performed by using OligoREADY Gold Nanopaticle Conjugation Kit (Cytodiagnostics Inc.). This kit has been optimized for high efficiency one-step conjugation of thiol-modified ssDNA directly to the Au-NPs surface. A TEM image of a ssDNA conjugated Au-NP is shown in the ESI (Fig. S1(b)†).

DNA assembly of Si-QDs and Au-NPs

For DNA hybridization, ssDNA modified Si-QDs and Au-NPs were mixed and heated in hybridization buffer (0.3 M NaCl, 10 mM phosphate (pH 7)).[50] The temperature was raised to 90 °C, held for 2 min, and then cooled down to room temperature with a rate of 2 °C min^{-1}.

Structural characterization

For IR absorption measurements (PerkinElmer, Spectrum GX), Si-QDs solution was drop-cast on a Au-coated Si substrate. Absorption spectra were obtained by a reflection-absorption geometry with the incident angle of 5° in dry air. The samples for TEM observations were prepared by dropping solutions onto carbon-coated copper grid. TEM, high angle annular dark-field scanning TEM (HAADF-STEM), and STEM-EDS mapping images were obtained by using JEM-2100F (JEOL) operating at 200 kV.

PL spectroscopy

PL spectra were measured using a spectrofluorometer (Flurolog-3, HORIBA Jovin Yvon) equipped with a photomultiplier (500–850 nm) and an InGaAs photodiode (800–1300 nm) or a single spectrometer equipped with a liquid nitrogen cooled InGaAs

diode array (OMA-V-SE, Roper Scientific). PL spectra obtained by different detectors were merged after correcting the sensitivity. The excitation source was a monochromatized Xe lamp (365 nm and 405 nm) or a semiconductor laser (405 nm). PL decay curves were obtained using image intensified CCD (ICCD) (PI-Max, Princeton Instrument). The excitation source was modulated 405 nm light. PL lifetimes were determined by $\tau = \int_{t_0}^{\infty} \left[\frac{I(t)}{I_0}\right] \mathrm{d}(t)$, where $I(t)$ is the PL intensity as a function of time t and I_0 is the initial intensity at time t_0. All the measurements were performed at room temperature.

Acknowledgements

This work is partly supported by 2014 JSPS Bilateral Joint Research Projects (Japan-Czech Republic), 2015 JST Visegrad Group (V4)-Japan Joint Research Project on Advanced Materials and KAKENHI (16H03828). HS acknowledges support from Grant-in-Aid for JSPS Fellows (# 26-3120).

Notes and references

1 W. C. W. Chan, D. J. Maxwell, X. Gao, R. E. Bailey, M. Han and S. Nie, *Curr. Opin. Biotechnol.*, 2002, **13**, 40–46.
2 X. Michalet, *Science*, 2005, **307**, 538–544.
3 M. Bruchez, M. Moronne, P. Gin, S. Weiss and a. P. Alivisatos, *Science*, 1998, **281**, 2013–2016.
4 X. Gao, Y. Cui, R. M. Levenson, L. W. K. Chung and S. Nie, *Nat. Biotechnol.*, 2004, **22**, 969–976.
5 U. Resch-Genger, M. Grabolle, S. Cavaliere-Jaricot, R. Nitschke and T. Nann, *Nat. Methods*, 2008, **5**, 763–775.
6 K. Fujioka, M. Hiruoka, K. Sato, N. Manabe, R. Miyasaka, S. Hanada, A. Hoshino, R. D. Tilley, Y. Manome, K. Hirakuri and K. Yamamoto, *Nanotechnology*, 2008, **19**, 415102.
7 F. Erogbogbo, K. Yong, I. Roy, R. Hu, W. Law, W. Zhao, H. Ding, F. Wu, R. Kumar, M. T. Swihart and P. N. Prasad, *ACS Nano*, 2011, **5**, 413–423.
8 M. Rosso-Vasic, E. Spruijt, Z. Popovic, K. Overgaag, B. van Lagen, B. Grandidier, D. Vanmaekelbergh, D. Dominguez-Gutierrez, L. De Cola and H. Zuilhof, *J. Mater. Chem.*, 2009, **19**, 5926–5933.
9 Y. Zhong, F. Peng, X. Wei, Y. Zhou, J. Wang, X. Jiang, Y. Su, S. Su, S. T. Lee and Y. He, *Angew. Chem., Int. Ed.*, 2012, **51**, 8485–8489.
10 Z. F. Li and E. Ruckenstein, *Nano Lett.*, 2004, **4**, 1463–1467.
11 J. H. Warner, A. Hoshino, K. Yamamoto and R. D. Tilley, *Angew. Chem.*, 2005, **117**, 4626–4630.
12 F. Erogbogbo, K. T. Yong, I. Roy, G. X. Xu, P. N. Prasad and M. T. Swihart, *ACS Nano*, 2008, **2**, 873–878.
13 Y. Zhong, F. Peng, F. Bao, S. Wang, X. Ji, L. Yang, Y. Su, S. T. Lee and Y. He, *J. Am. Chem. Soc.*, 2013, **135**, 8350–8356.
14 B. F. P. Mcvey and R. D. Tilley, *Acc. Chem. Res.*, 2014, **47**, 3045–3051.
15 F. Erogbogbo, C. A. Tien, C. W. Chang, K. T. Yong, W. C. Law, H. Ding, I. Roy, M. T. Swihart and P. N. Prasad, *Bioconjugate Chem.*, 2011, **22**, 1081–1088.
16 X. Cheng, S. B. Lowe, P. J. Reece and J. J. Gooding, *Chem. Soc. Rev.*, 2014, **43**, 2680.
17 M. Montalti, a. Cantelli and G. Battistelli, *Chem. Soc. Rev.*, 2015, **44**, 4853–4921.
18 J. Choi, N. Sun Wang and V. Reipa, *Bioconjugate Chem.*, 2008, **19**, 680–685.
19 L. Wang, V. Reipa and J. Blasic, *Bioconjugate Chem.*, 2004, **15**, 409–412.
20 R. Intartaglia, A. Barchanski, K. Bagga, A. Genovese, G. Das, P. Wagener, E. Di Fabrizio, A. Diaspro, F. Brandi and S. Barcikowski, *Nanoscale*, 2012, **4**, 1271–1274.
21 L. Ruizendaal, S. P. Pujari, V. Gevaerts, J. M. J. Paulusse and H. Zuilhof, *Chem.–Asian J.*, 2011, **6**, 2776–2786.
22 D. Kovalev, H. Heckler, G. Polisski and F. Koch, *Phys. Status Solidi*, 1999, **215**, 871–932.
23 S. Takeoka, M. Fujii and S. Hayashi, *Phys. Rev. B: Condens. Matter Mater. Phys.*, 2000, **62**, 16820–16825.
24 M. Dasog, Z. Yang, S. Regli, T. M. Atkins, A. Faramus, M. P. Singh, E. Muthuswamy, S. M. Kauzlarich, R. D. Tilley and J. G. C. Veinot, *ACS Nano*, 2013, **7**, 2676–2685.
25 A. Shiohara, S. Hanada, S. Prabakar, K. Fujioka, T. H. Lim, K. Yamamoto, P. T. Northcote and R. D. Tilley, *J. Am. Chem. Soc.*, 2010, **132**, 248–253.
26 X. Cheng, R. Gondosiswanto, S. Ciampi, P. J. Reece and J. J. Gooding, *Chem. Commun.*, 2012, **48**, 11874–11876.
27 K. Dohnalová, A. N. Poddubny, A. a Prokofiev, W. D. de Boer, C. P. Umesh, J. M. Paulusse, H. Zuilhof and T. Gregorkiewicz, *Light: Sci. Appl.*, 2013, **2**, e47.
28 M. Dasog, G. B. De Los Reyes, L. V. Titova, F. A. Hegmann and J. G. C. Veinot, *ACS Nano*, 2014, **8**, 9636–9648.
29 R. D. Tilley, J. H. Warner, K. Yamamoto, I. Matsui and H. Fujimori, *Chem. Commun.*, 2005, 1833–1835.
30 J. H. Warner, H. Rubinsztein-Dunlop and R. D. Tilley, *J. Phys. Chem. B*, 2005, **109**, 19064–19067.
31 J. V. Frangioni, *Curr. Opin. Chem. Biol.*, 2003, **7**, 626–634.
32 H. Sugimoto, M. Fujii, K. Imakita, S. Hayashi and K. Akamatsu, *J. Phys. Chem. C*, 2012, **116**, 17969–17974.
33 H. Sugimoto, M. Fujii, Y. Fukuda, K. Imakita and K. Akamatsu, *Nanoscale*, 2014, **6**, 122–126.
34 H. Sugimoto, M. Fujii, K. Imakita, S. Hayashi and K. Akamatsu, *J. Phys. Chem. C*, 2013, **117**, 11850–11857.
35 H. Sugimoto, M. Fujii and K. Imakita, *Nanoscale*, 2016, **8**, 10956–10962.
36 H. Naiki, A. Masuhara, S. Masuo, T. Onodera, H. Kasai and H. Oikawa, *J. Phys. Chem. C*, 2013, **117**, 2455–2459.
37 N. Liu, B. S. Prall and V. I. Klimov, *Langmuir*, 2006, **128**, 15362–15363.
38 S. E. Park, M. Y. Park, P. K. Han and S. W. Lee, *Bull. Korean Chem. Soc.*, 2006, **27**, 1341–1345.
39 D. V. Quang, J. K. Kim, P. B. Sarawade, D. H. Tuan and H. T. Kim, *J. Ind. Eng. Chem.*, 2012, **18**, 83–87.
40 S. A. Kulkarni, S. B. Ogale and K. P. Vijayamohanan, *J. Colloid Interface Sci.*, 2008, **318**, 372–379.
41 X. Cheng, S. B. Lowe, P. J. Reece and J. J. Gooding, *Chem. Soc. Rev.*, 2014, **43**, 2680–2700.
42 M. Kunishima, C. Kawachi, K. Hioki, K. Terao and S. Tani, *Tetrahedron*, 2001, **57**, 1551–1558.

43 E. Cohen-Hoshen, G. W. Bryant, I. Pinkas, J. Sperling and I. Bar-Joseph, *Nano Lett.*, 2012, **12**, 4260–4264.
44 X. Ma, K. Fletcher, T. Kipp, M. P. Grzelczak, Z. Wang, I. Pastoriza-santos, A. Kornowski and L. M. Liz-marz, *J. Phys. Chem. Lett.*, 2011, **2**, 2466–2471.
45 N. A. Harun, M. J. Benning, B. R. Horrocks and D. a. Fulton, *Nanoscale*, 2013, **5**, 3817–3827.
46 J. Lee, A. O. Govorov, J. Dulka and N. a. Kotov, *Nano Lett.*, 2004, **4**, 2323–2330.
47 H. Sugimoto, M. Fujii, Y. Fukuda, K. Imakita and K. Akamatsu, *Nanoscale*, 2014, **6**, 122–126.
48 M. P. Busson, B. Rolly, B. Stout, N. Bonod, E. Larquet, A. Polman and S. Bidault, *Nano Lett.*, 2011, **11**, 5060–5065.
49 N. G. Bastus, J. Comenge and V. Puntes, *Langmuir*, 2011, **27**, 11098–11105.
50 R. Jin, G. Wu, Z. Li, C. A. Mirkin and G. C. Schatz, *J. Am. Chem. Soc.*, 2003, **125**, 1643–1654.